High-Gain Single-Feed Overmoded Cavity Antenna with Closely-Spaced Phased Patch Surface

Shu-Lin Chen, *Member, IEEE,* Yanhui Liu, *Senior Member, IEEE,* Richard W. Ziolkowski, *Life Fellow, IEEE* Zheng Li, *Member, IEEE,* and Y. Jay Guo, *Fellow, IEEE*

***Abstract*—High-gain single-feed antennas are desired for current and future wireless systems. Slot-based highly overmoded cavity antennas are one solution, but the fact that they can only radiate broadside beams limits their applications. An innovative phase-control technique is developed for slot-based resonant cavity antennas that utilizes a planar array of closely-spaced, appropriately-sized metallic patches integrated into the very near field of their slot arrays. It facilitates the design and realization of the phase distribution over their radiating aperture that is required for them to generate single and/or multiple tilted beams pointed at specified directions. A $\mathrm{TE}_{(10)(11)(0)}$-mode slot-based cavity antenna is selected as the pathfinder system. A TE_{110}-mode single-slot cavity antenna that is equivalent to the half-wavelength subsection of that cavity is introduced initially to monitor the phase radiated from each slot. The phase control surface is then carefully engineered to facilitate tilted output beams from the base design. The approach is validated with two subsequent tilted-beam systems. The first system achieves a single beam tilted to 30° with respect to the broadside direction. The second system is extended to produce two independently-directed titled beams pointing at -10° and 20°, respectively. All of the measured results agree well with their simulated values.**

***Index Terms*—Cavity antenna, directed beams, high gain, phase control, resonant modes.**

I. Introduction

HIGHLY directive antennas are promising candidates for current and future wireless systems that desire high data rates, stable quality links, and low costs [1]–[4]. Generally, they can direct and confine radiated power to specific regions, i.e., to form focused high-gain radiation patterns. In order to facilitate this specified pattern characteristic, antennas must be equipped with an effective beam-forming technique.

One option has been to employ an array of individual radiating elements with separate feeds [5]–[7] or a single feed using a power-distribution network [8]–[12]. In contrast, several notable antenna techniques have been reported to control a large surface to produce highly directive beams. Transmitarray (reflectarray) antennas introduce a focal source to spatially illuminate a transmitarray (reflectarray) surface with an appropriate focus-to-diameter (F/D) ratio [13]–[21]. Their overall profiles usually are comparable to achieve a high-gain beam having a similar aperture diameter (D) and high F/D value. A single-feed cavity-excited Huygens' metasurface antenna was reported in [22] that realized a highly directive beam with a high aperture efficiency. However, its profile is high, usually being larger than one wavelength. Fabry-Perot (FP) antennas [23]–[27], modulated surface antennas [28], [29], and radial-line slot antennas [30]–[32] have been employed for high-gain patterns arising from low-profile systems. They typically radiate through leaky waves on their surfaces that are excited by a single source in the center. As is commonly known, there is a compromise between edge losses and aperture efficiency for those leaky-wave antennas.

Slot-based higher-order-mode cavity antennas that radiate through their resonant cavity modes can avoid the aforementioned edge losses. They also exhibit other substantial benefits, e.g., being low in profile, having simple configurations and exhibiting high gain [33]–[36]. A TE_{440} mode was excited in the cavity developed in [35]. A total of 16 slots was appropriately etched to achieve a system that radiated a broadside beam with a gain of around 16.0 dBi. A W-band TE_{560}-mode substrate-integrated cavity antenna was employed as the radiating element in 4×4 and 8×8 arrays in [36] to obtain broadside beams with measured peak gains of 26.39 and 30.36 dBi, respectively. On the other hand, only broadside-beam patterns were achieved with all of these reported higher-order-mode cavity antennas. This limitation is caused by an inherent property of a resonant cavity mode, i.e., the dependence of the resonance on the cavities physical properties makes it difficult to implement a specific phase variation on each of its radiating slots. Consequently, it is challenging to produce a high-gain tilted beam from slot-based higher-order-mode cavity antennas. Nevertheless, high-gain tilted-beam patterns are necessary for many applications dealing, for example, with unmanned aerial vehicle (UAV) communications.

To address this challenge, we have developed an innovative phase control technique to achieve tilted beams from slot-based highly overmoded cavity antennas. This enhanced functionality is attained through the introduction of a surface of closely-spaced, appropriately-sized metallic patches positioned above the properly-offset radiating slots etched in the upper surface of a rectangular air-filled cavity. There are three significant aspects of this work. First, we present an original method to control the phases of the fields radiated by a slot-based resonant overmoded cavity antenna. A metallic patch surface is introduced into the very near field of the cavity antenna's slot array to achieve this control.

Manuscript received XXX. This work was supported by the Australian Research Council (ARC) Discovery Project (DP) 160102219 grant. *(Corresponding author: Yanhui Liu)*

S.-L. Chen, Y. Liu, R. W. Ziolkowski and Y. J. Guo are with the Global Big Data Technologies Centre (GBDTC), University of Technology Sydney (UTS), Ultimo, NSW 2007, Australia. (E-mail: Shulin.Chen@uts.edu.au; yhliu@uestc.edu.cn; Richard.Ziolkowski@uts.edu.au; Jay.Guo@uts.edu.au)

Y. Liu is also with the School of Electronic Engineering, University of Electronic Science and Technology of China, Chengdu 610054, China.

Z. Li is with the Institute of Lightwave Technology, Beijing Jiaotong University, Beijing 100044, China. (E-mail: lizheng@bjtu.edu.cn)

Second, an analysis method is developed based on a unit cavity antenna model, i.e., a single-slot TE_{110}-mode cavity antenna. It overcomes the difficulties associated with trying to extract the phase associated with a single slot from the composite fields radiated by the entire $TE_{(10)(11)(0)}$-mode slot-based resonant cavity antenna. Relationships among the single element's phase, patch length, and slot offset are established. They are used to optimize the performance characteristics of the overall system. Finally, a simple, yet very effective, high-gain tilted beam configuration is realized for this slot-based overmoded resonant cavity antenna augmented with the near-field metallic-patch surface. Two high-gain tilted-beam antenna systems are designed with this approach. One radiates a single tilted beam with a realized gain of 25.3 dBi; the other radiates two tilted high gain beams whose beam angles can be independently specified. We note that the beam-tilt range of the final patch-augmented systems is dependent on the electrical distance between their slot elements. Both antennas have a low profile of around $0.4\lambda_0$. Their prototypes were fabricated and tested successfully, confirming their simulated performance characteristics.

II. Phase Control for Overmoded Cavity Antenna

The base design, a slot-based $TE_{(10)(11)(0)}$-mode cavity antenna, is described. This highly overmoded system is regarded equivalently as a 10×11 "slot element" array. A TE_{110}-mode single-slot cavity antenna, basically one subsection of the array, is introduced to understand the radiation performance of each slot element. A metallic patch is introduced above this antenna. The phase of the fields it radiates into the far field is monitored as the patch's shape and the offset of the slot over which it is closely placed are explored.

A. Overmoded Cavity Antenna

A side view of the slot-based $TE_{(10)(11)(0)}$-mode cavity antenna is shown in Fig. 1. It consists of a single-layer copper-clad substrate, an air-filled rectangular cavity, and a standard WR-90 rectangular waveguide feed. The substrate is F4BM-2 produced by Wangling Company, China. It has a permittivity of ε_r = 2.2, a loss tangent of $\tan\delta$ = 0.001, and a height of h_s = 0.5 mm. Its top metal surface is removed completely, and a slot layer is printed on its bottom surface. The rectangular cavity is formed with aluminum pieces. The top view of its bottom and sides is depicted in Fig. 2. It has the length L_c, width W_c, and height h_c. The height h_c is very small in terms of wavelength and, hence, the electric-field (E-field) magnitude can be regarded approximately as invariant along the z-axis. Note that a square hole with dimensions of $L_h \times L_h \times h_b$ is drilled for the impedance transition between the WR-90 waveguide feed and the antenna. Screw holes, 24 in total, are drilled around the edges of both the substrate and the cavity prototype to allow for assembling the antenna.

Fig. 3 gives the top view of the magnitude of the simulated E-field distribution of the $TE_{(10)(11)(0)}$ standing wave mode excited in the rectangular cavity at 10.5 GHz. One observes that there are 10 half-wavelength sections along the x-axis and 11 along the y-axis. The position of the center of the waveguide feed was selected to be at the center point of the rectangular cavity as depicted. A top view of the waveguide feed is illustrated in the top right inset. Its long side is placed parallel to the y-axis, and its narrow side is aligned with the x-axis.

Fig. 4 shows the top view of the slot layer. It is a metallic sheet with 110 slots, i.e., 10 rows and 11 columns, etched into it. Each slot has the same length L_t and width W_t. A close-up view of four adjacent, resonant half-wavelength subsections of the antenna and the E-field distributions beneath their slots is given on the top right inset. As depicted, each slot is offset a distance d_0 along either the $+$y-axis or $-$y-axis with respect to the vertical center line of each subsection. Moreover, the slots in any two adjacent subsections are offset from their centers in opposite directions. This well-known choice properly compensates for the out-of-phase E-fields

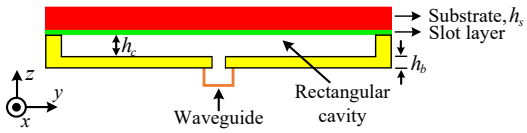

Fig. 1. Side view of the slot-based overmoded rectangular cavity antenna. (h_c = 4 mm and h_b = 2 mm)

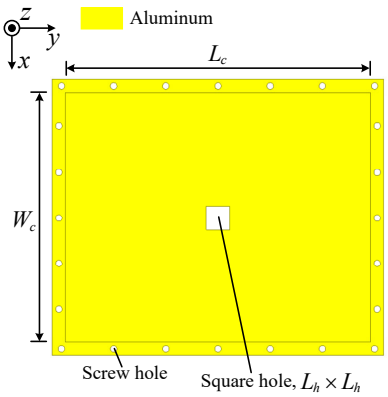

Fig. 2. Top view of the bottom and sides of the rectangular cavity of the prototype. A square hole in its bottom surface is noted. (L_c = 234 mm, W_c = 192 mm, and L_h = 18 mm)

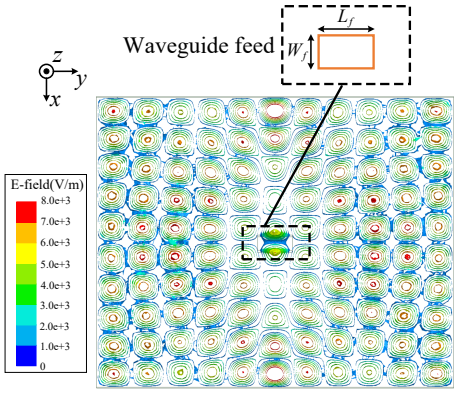

Fig. 3. Top view of the E-field magnitude of the simulated $TE_{(10)(11)(0)}$ standing wave mode excited inside the rectangular cavity at 10.5 GHz by the rectangular waveguide feed.

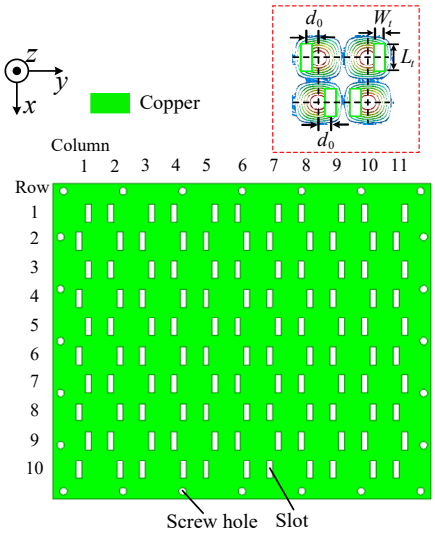

Fig. 4. Top view of the slot layer located on the bottom of the substrate. A close-up view of four adjacent slots with resonant half-wavelength subsections is given in the top right inset. ($d_0 = 1.5$ mm, $L_t = 10$ mm, $W_t = 3$ mm)

in them. It thus leads to an in-phase superposition of the fields radiated by all of the slots, and makes the slot-based overmoded rectangular cavity antenna equivalent to an array with 10×11 in-phase "slot elements".

B. TE_{110}-Mode Single-Slot Cavity Antenna

In order to realize high-gain tilted-beam patterns from an overmoded cavity antenna, the phase distribution of the fields radiated by all of the slots must be controlled. This requires knowing the phase of the fields radiated by each slot element separately, which is a difficult property to extract from the composite field. This challenging requirement is met by determining the radiation performance and, hence, the phase response of an arbitrary element in the overall slot array etched on the top surface of the $TE_{(10)(11)(0)}$-mode cavity. As previously noted, only one slot exists over each resonant half-wavelength subsection of the cavity, and the E-fields on the four sides of this subsection are close-to-zero. One can approximately replace those sides with perfect-electric-conductors (PECs) and, thus, attain a single slot etched on a TE_{110}-mode cavity. This configuration thus isolates the slot element and allows an investigation of the radiation performance of this equivalent single-slot resonant TE_{110}-mode cavity antenna.

The dimensions of the TE_{110}-mode single-slot cavity are thus: $W_e = 19.2$ mm, and $L_e = 21.27$ mm. Fig. 5(a) shows a side view of this TE_{110}-mode single-slot cavity antenna. Fig. 5(b) shows the top view of its slot layer. Since the dimensions of the WR-90 waveguide are comparable to those of the TE_{110}-mode single-slot cavity antenna, it is not an appropriate feed for this antenna. Consequently, a coaxial line was selected to excite it. The position of this coaxial feed (in millimeters): $x_f = 3$, $y_f = 4.5$, was optimized to excite the desired TE_{110} mode.

This TE_{110}-mode single-slot cavity antenna was simulated with the ANSYS high frequency structure simulator (HFSS) software. Simulations indicate that the TE_{110} mode, i.e., the mode in which one half-wavelength is along both the x- and y-axes, has been successfully produced at 10.5 GHz in the cavity. A broadside beam with a gain value of 3.7 dBi is achieved.

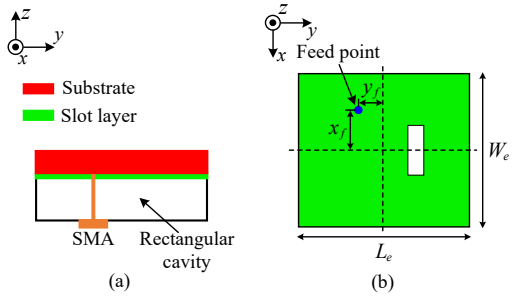

Fig. 5. Configuration of the TE_{110}-mode single-slot cavity antenna. (a) Side view. (b) Top view of its slot layer.

C. Phase Control Mechanism

A means to control the phase of the fields radiated by the TE_{110}-mode single-slot cavity antenna was sought. One finds it impractical to introduce perturbations in the cavity without deteriorating the mode distribution. Consequently, an innovative near-field phase control technique was developed for slot-based resonant cavity antennas. It relies on positioning a metallic patch array in the very near field of their radiating aperture with only a single patch being located above one element of the slot array. Fig. 6(a) depicts a side view of the single-slot cavity antenna augmented with this metallic patch. The patch is printed on the bottom of another piece of the 0.5 mm thick F4BM-2 substrate and is located above the slot and close to it. The two substrates are separated by an air gap whose height is h_a. Fig. 6(b) shows the top view of the patch-augmented antenna without both of the substrates being present. The metallic patch is symmetrically located with respect to the slot center, and its size is labeled as $L_p \times W_p$.

Generally, the phase behavior of a unit element of an array is investigated by illuminating it with a plane wave [13], [23], [37]. Unfortunately, this method is not feasible for the patch-augmented single-slot cavity antenna since its particular TE_{110}-mode fields would not be excited well. However, we can

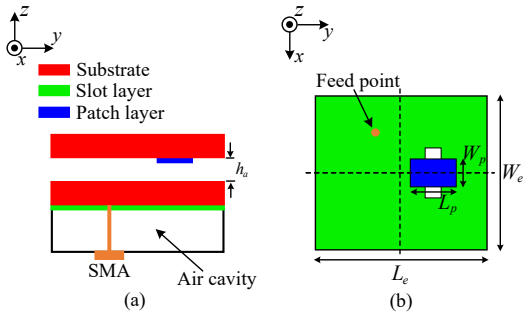

Fig. 6. Configuration of the single-slot cavity antenna augmented with a metallic patch located above the slot and spaced close to it. (a) Side view. (b) Top view without both of its substrates being present.

use HFSS to monitor the phase of the simulated far-field E-fields that the patch-augmented slot radiates when the TE_{110}-mode cavity antenna is excited by a coaxial feed.

The near-field distribution radiated by the slot is tightly coupled to the nearby patch and strongly excites its edges. A broadside-beam pattern is again formed in the far field. Monitoring its phase as the size of the patch and the air gap height are varied, it was concluded that the slot-coupled patch acts as a phase delay element for the fields radiated from the slot. The capacitive coupling between the slot and the closely-spaced patch is crucial to modifying the resulting far-field phase behavior. Although configurations that employ augmented patches loaded above a slot-based resonant cavity were reported in [38], [39], their operating mechanisms are quite different. They employed the slots to couple energy directly to the patches because they serve as the main radiators, not the slots. Consequently, the patch length is generally half of the wavelength of the operating frequency [38]–[42]. Furthermore, the slots of those systems were etched uniformly into the cavity rather than having them associated with each half-wavelength subsection and oppositely positioned in adjacent ones as is done here. Thus, their patches only are present to improve the broadside radiation performance of those systems.

D. Parameter Study and Analysis

Parameter studies of the three main design dimensions, i.e., the patch length L_p, patch width W_p, and air gap h_a, were considered. They mainly affect the aforementioned capacitive coupling and, hence, the associated far-field phase behavior. Initial values for the parameters were selected as (in millimeters): $L_p = 6.0$, $W_p = 6.0$, $h_a = 2.5$.

Fig. 7 shows the simulated phase and gain values of the E-field at broadside as the patch length L_p is varied. It is observed that when L_p increases from 1 to 5 mm, the phase value is decreased from 196.1° to 167.6°, i.e., a 28.5° variation, and the gain value is increased from 2.4 to 4.9 dBi. When the value of L_p is increased further to 9 mm, the phase value continuously decreases to 80.4° while the gain values vary between 3 and 5.5 dBi. When L_p varies from 9 to 13 mm, the phase value stably reduces from 80.4° to 64.2°, and the gain value also reduces from 3 to −4.3 dBi. One finds that a total of 131.9° phase variation range is obtained by varying L_p. The fastest phase variation occurs when L_p is varied between 5 and 9 mm.

The parameter study of the patch width W_p shows that the phase variation range is only 39.2° when W_p is varied from 1 to 10 mm. The corresponding parameter study of the air gap h_a shows that the phase value stably increases from 58.7° to 168.3°, i.e., a 109.6° variation, when it varies from 1 to 6 mm. While it is rather difficult to realize accurate variation of air gap h_a for phase control in practical applications, changes to the patch's length L_p and width W_p are easily implemented. With the knowledge that the largest phase variation range is 131.9°, i.e., from 64.2° to 196.1°, by varying L_p, it was decided to alter a combination of L_p and W_p to extend the phase variation range. Nevertheless, it is found that when the maximum (minimum) phase value of 196.1° (64.2°) was chosen, i.e., L_p = 1 mm (13 mm), the phase value obtained by changing W_p could not be further increased (decreased). This outcome indicated that the phase variation range could not be broadened simply with this combination approach. Consequently, it was decided for simplicity to only vary the patch length L_p to control the far-field phase.

Unfortunately, the 131.9° phase variation range is not large enough to realize focused tilted beam patterns. It was found that by reversing the offset location of the slot relative to the center of the antenna and by moving the patch to be again directly over it doubles the phase variation range. Fig. 8 shows the top view of the patch-augmented single-slot cavity antenna with opposite offsets of the slot and patch. Recalling that the slot offsets occur in opposite directions in the full array because the E-fields are out-of-phase between adjacent subsections, the far-field phases associated to the fields radiated by adjacent subsections will also have this 180° phase difference. Since a phase variation range from 64.2° to 196.1° can be achieved by varying the patch length of the $+y$-axis slot-offset antenna shown in Fig. 8(a), the attainable phase value range from the $-y$-axis slot-offset antenna shown in Fig. 8(b) is then from −115.8° to 16.1°. Consequently, a phase variation range totaling 263.8° can be achieved by properly selecting the patch lengths and the slot offsets for the elements in the full array.

A database of discrete phase values (Φ_p) was compiled from these parameter studies. It is summarized in Table I. Note that all of the phase values have been normalized to the one obtained when L_p = 1 mm. The maximum phase inaccuracy caused by the necessary practical discretization of the patch lengths that occurs between the phase values corresponding to

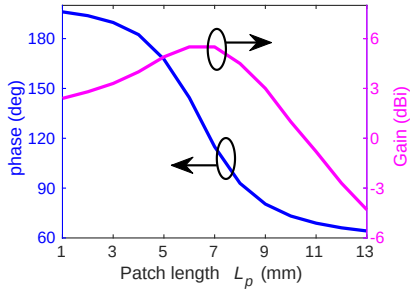

Fig. 7. The simulated phase and gain values of the E-field at broadside as the patch length L_p is varied.

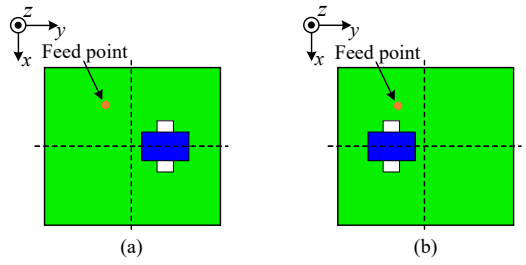

Fig. 8. Top view of the patch-augmented single-slot cavity antenna with opposite offsets of the slot. (a) Offset along the $+y$-axis. (b) Offset along the $-y$-axis.

TABLE I
DATABASE OF DISCRETE PHASE VALUES

L_p (mm)		1	5	6	6.5	7	8	9.5	13
Φ_p (°)	$+y$	0	−27.9	−51.9	−66.1	−81.1	−103.3	−119.8	−131.9
	$-y$	180	152.1	128.1	113.9	98.9	76.7	60.2	48.1

"$+y$" denotes slot offset along $+y$ axis

"$-y$" denotes slot offset along $-y$ axis

L_p = 1 and L_p = 5 mm is $27.9°/2 = 13.45°$. There are also phase gaps between the two obtained phase variation ranges, i.e., $-131.9°$ to $0°$ and $48.1°$ to $180°$. The corresponding maximum phase inaccuracy is $48.1°/2 = 24.05°$. Simulations confirmed that these inaccuracies have little effect on the realized performance of the entire array.

III. OVERMODED CAVITY ANTENNA WITH TILTED-BEAM PATTERNS

The desired tilted-beam functionality of a slot-based highly overmoded cavity antenna is accomplished by introducing a phase control surface to achieve the necessary phase distribution over the entire slot array. To illustrate the ensuing tilted beam functionality with the slot-based $TE_{(10)(11)(0)}$-mode cavity antenna, we have elected to realize 1-D tilted patterns in zx-plane (H-plane). Note that the necessary offsets and patch lengths then make the array non-uniform along the y-axis. Two examples are presented that were optimally designed to radiate, respectively, a single tilted beam and two independently-directed tilted beams.

A. Overmoded Cavity Antenna with a Single Tilted Beam

Consider an N-element uniform linear array placed along the x-axis. It is well-known that one can impose a progressive phase Φ_n on n-th element to realize a focused beam pointing at an angle θ_0. This phase value can be calculated as [5]:

$$\Phi_n = \angle e^{-j(n-1)kd\sin\theta_0} \tag{1}$$

where k is the propagation constant in air, d is the distance between two adjacent elements, and "$\angle$" is the function that returns the phase angle in degrees.

The main beam angle θ_0 was selected as 30°, i.e., the patch-augmented slot-based $TE_{(10)(11)(0)}$-mode cavity antenna is designed to radiate a beam tilted at 30° from broadside in zx plane. It requires the determination of the appropriate offset of each slot in the base design as well as the proper length of the corresponding patches in the phase-control surface. The 10 patch-augmented slot elements in the first column are engineered to attain the required phase variation. The phase of the first element is chosen as the reference, i.e., $\Phi_1 = 0$. Its patch length L_p = 1 mm and the offset of the slot over which it is placed is "$+y$", i.e., along $+y$-axis. Then the process used to determine the patch length L_p and slot offset for the n-th ($n \geq 2$) element in column one is summarized as follows:

1) Noting that the phase Φ_n is a value between $-180°$ and 180°, one can calculate it by substituting the design parameter values into (1).
2) If the calculated $\Phi_n \in (-155.95°, 180°]$, one should compare Φ_n with all of the 16 phase values of Φ_p provided in Table I. One then finds the Φ_p such that $|\Phi_p - \Phi_n|$ attains its minimum value. Otherwise, if $\Phi_n \in [-180°, -155.95°]$, then Φ_p is 180°.
3) The patch length L_p that corresponds to this Φ_p is the desired one.
4) If $\Phi_p > 0$, when n is an odd (even) number, the slot offset should be "$-y$" ("$+y$").
5) if $\Phi_p \leq 0$, When n is an odd (even) number, the slot offset should be "$+y$" ("$-y$").

The phase values Φ_n of the n-th element obtained when θ_0 = 30° are shown in the second row of Table II. The determined patch lengths and slot offsets are given in the last two rows. Subsequently, one can calculate the theoretical co-polarization (co-pol.) pattern for the 10-element linear array. The phase associated with each element is chosen as the phase value Φ_p that corresponds to its patch length L_p. The element pattern then is the co-pol. gain pattern of the patch-augmented single-

TABLE II
VALUES FOR THE PATCH-AUGMENTED OVERMODED CAVITY ANTENNA WITH A SINGLE TILTED BEAM

Element	1	2	3	4	5	6	7	8	9	10
Φ_n (°)	0	−120.8	118.4	−2.3	−123.1	116.1	−4.7	−125.5	113.8	−7.0
L_p (mm)	1	9.5	6.5	1	9.5	6.5	1	9.5	6.5	1
Offset	$+y$	$-y$	$-y$	$-y$	$+y$	$+y$	$+y$	$-y$	$-y$	$-y$

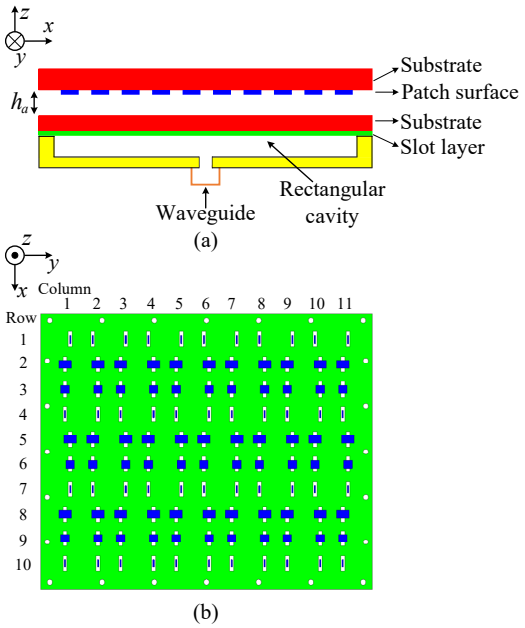

Fig. 9. Configuration of the slot-based overmoded rectangular cavity antenna that radiates a single tilted beam. (a) Side view. (b) Top view without its substrates being present.

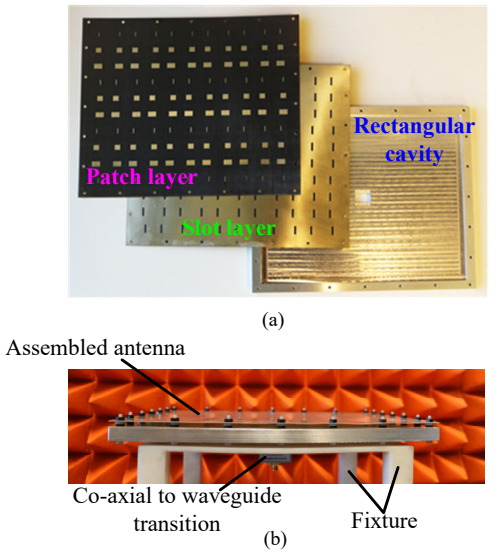

Fig. 10. Photos of the fabricated antenna prototype. (a) Before assembly. (b) Assembled antenna in the measurement chamber.

slot cavity antenna with the corresponding patch length L_p.

The other ten columns employ the same patches as those in the first column. Opposite offsets of the slots are utilized between two adjacent columns to maintain the in-phase far-field superposition. The antenna represents a simple and efficient tilted beam design, i.e., the slot-based overmoded cavity excites the phase control surface to realize the desired high-gain tilted-beam pattern. It was simulated, fabricated and tested. Its side and top views are shown in Fig. 9(a) and (b), respectively. The design parameter values of the final system are (in millimeters): L_t = 9.5, W_t = 2, h_a = 4.5, while all of the others are fixed to be the same as the base design. The antenna's profile is 11.5 mm (around $0.4\lambda_0$), where λ_0 is the free-space wavelength at 10.5 GHz.

Figs. 10(a) and (b) show photos of the fabricated prototype before and after assembly, respectively. The antenna's simulated and measured S-parameters are presented in Fig. 11. The measured results are in good agreement with their simulated values. The measured $|S_{11}| \leq -10$ dB bandwidth is 30 MHz, from 10.48 to 10.51 GHz. This narrow bandwidth is associated with the fact that the antenna is resonant and operating with the very high-order mode of its cavity, which has a very high quality-factor (Q-factor) [43].

The theoretical, simulated, and measured co-pol. normalized radiation patterns in the zx-plane at 10.5 GHz are shown in Fig. 12. It is observed that all of the theoretical, simulated, and measured co-pol. patterns agree very well, and their main beams point towards the specified 30° from the broadside direction. The simulated peak realized gain value is 26.2 dBi at 10.5 GHz while the measured one is 25.3 dBi. The antenna's simulated radiation efficiency is 96.2% at 10.5 GHz, which indicates that the ohmic losses associated with it are very small. Moreover, both the simulated and measured cross-polarization (x-pol.) levels are very low, the measured x-pol. level being lower than −36.8 dB. These results confirm the effectiveness of the developed phase-control surface to

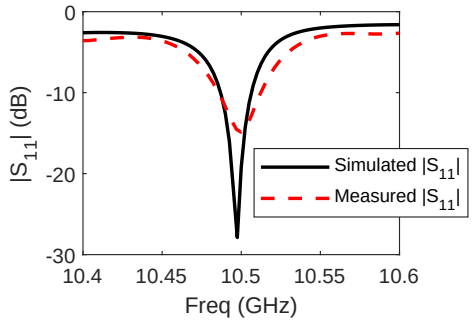

Fig. 11. Simulated and measured S-parameters of the patch-augmented slot-based overmoded cavity antenna with a single tilted beam.

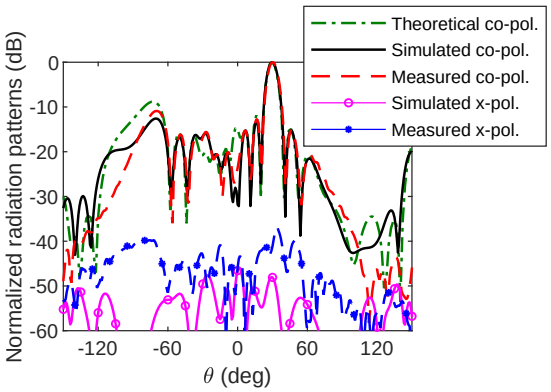

Fig. 12. Theoretical, simulated, and measured normalized radiation patterns of the single-beam, patch-augmented slot-based overmoded rectangular cavity antenna at 10.5 GHz.

enable the realization of high-gain tilted beams from slot-based overmoded cavity antennas.

One also finds a second lobe near −72° for the theoretical co-pol. radiation pattern that is −8.8 dB lower than the main lobe. It is a grating lobe [44], which arises because the distance between the radiating elements is larger than half of the free space wavelength at the operating frequency. One possible solution to lower or even remove it would be to fill the air cavity with a dielectric substrate. This would allow for a decrease in the element spacing because the wavelength in the dielectric would be smaller while not impacting the free space wavelength. However, the tradeoff would be some decrease in the overall efficiency because there would then be additional losses in the substrate. Another option would be to load a carefully-designed metasurface to equivalently reduce the spacing between the radiating elements.

Note that the theoretical calculation did not take into account any mutual coupling and edge effects. The grating lobe level is consequently higher than that obtained with the HFSS simulation, −12.6 dB. The measured value is around −11.0 dB. The small discrepancy between the simulated and measured results is very reasonable given fabrication inaccuracies. While the measured grating lobe value is a bit higher than the theoretical first sidelobe level of a uniform linear array, −13.46 dB, it is nevertheless quite acceptable for many applications. Moreover, it occurs well away from the tilted beam's direction.

B. Overmoded Cavity Antenna with Two Independently-Directed Tilted Beams

While single tilted beams are useful, antennas that radiate multiple independently-directed high-gain beams are of recognized importance for fifth generation (5G) systems dealing with point-to-multipoint applications. The realized phase-control surface augmented slot-based overmoded cavity antenna with two independently-directed tilted beams described below is considered to be an initial step to address that need. Being able to point the two beams independently at two specified angles greatly increases the usefulness of the system.

TABLE III
VALUES FOR THE PATCH-AUGMENTED OVERMODED CAVITY ANTENNA WITH TWO INDEPENDENTLY-DIRECTED TILTED BEAMS

Element	1	2	3	4	5	6	7	8	9	10
Φ_n (°)	0	−20.3	139.3	119.0	98.6	−101.7	−122.0	−142.4	17.3	−3.0
L_p (mm)	1	5	6	6.5	7	8	9.5	13	1	1
Offset	$+y$	$-y$	$-y$	$+y$	$-y$	$-y$	$+y$	$-y$	$+y$	$-y$

The two main beams are specified to point towards $\theta_1 = -10°$ and $\theta_2 = 20°$, respectively. A more complex phase value Φ_n can be defined for the n-th element to achieve these two desired beams:

$$\Phi_n = \angle(e^{-j(n-1)kd\sin\theta_1} + e^{-j(n-1)kd\sin\theta_2}) \qquad (2)$$

Substituting the array parameter values into (2), the requisite phase Φ_n for the for the n-th element was calculated and is shared in the second row of Table III. Using the aforementioned phase determination process, the augmented patch lengths as well as the slot offsets for the 10 elements in the first column were obtained and are given in the last two rows of Table III. The top view of the realized two-beam system is shown in Fig. 13 without the substrates being present.

Fig.14 compares the simulated and measured S-parameters. The measured −10 dB bandwidth is 20 MHz, ranging from 10.48 to 10.5 GHz. Fig. 15 shows the theoretical, simulated, and measured normalized radiation patterns in zx plane. Again, these results agree well with each other. The measured (simulated) two main beams, respectively, point towards −9° (−10°) and 21° (20°). The minor shifts of the measured and simulated main-beam angles are again caused by an accumulation of minor fabrication inaccuracies. The antenna's simulated radiation efficiency is 98.1% at 10.5 GHz, again indicating very small ohmic losses. The measured (simulated) peak realized gain value is 23.9 dBi (24.3 dBi) for the main beam pointing towards −9° (−10°). The corresponding measured (simulated) peak value is 22.7 dBi (23.1 dBi) at the other main beam angle, 21° (20°). The measured x-pol. levels are all lower than −38 dB.

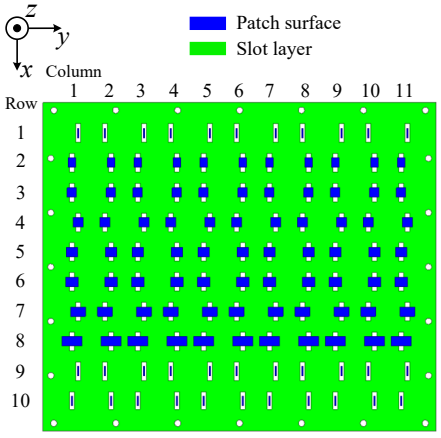

Fig. 13. Top view of the overmoded rectangular cavity antenna that radiates two independently-directed tilted beams without its substrates being present.

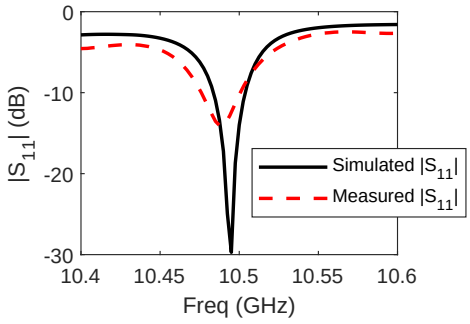

Fig. 14. Simulated and measured S-parameters of the patch-augmented slot-based overmoded cavity antenna with two independently-directed tilted beams.

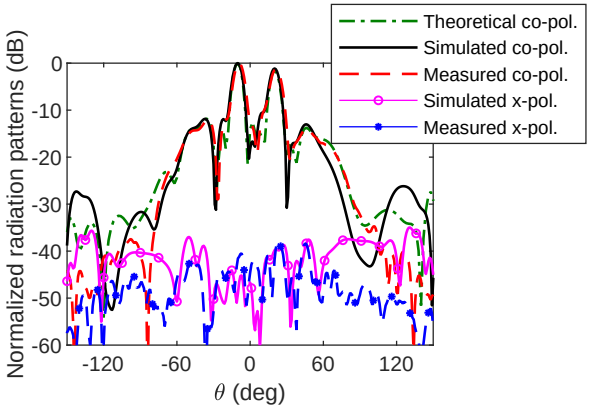

Fig. 15. Theoretical, simulated, and measured normalized radiation patterns of the dual-beam, patch-augmented slot-based overmoded rectangular cavity antenna at 10.5 GHz.

IV. DISCUSSION

A. Comparison

A detailed comparison of the antenna developed in this work and other previously reported antennas is given in Table IV. Various techniques have been reported that can realize high-gain tilted beams. Transmitarray/reflectarray antennas and Fabry-Perot cavity antennas can obtain a wide operating frequency bandwidth, but their profiles are high, e.g., larger than $1.4\lambda_0$, as reported in [18], [20], and [26]. The other structures, i.e., the modulated metasurface in [28] and radial line slot in [30], as well as the overmoded cavity considered in this work, yield antennas that operate with very narrow

TABLE IV
DETAILED COMPARISON BETWEEN THE ANTENNA DEVELOPED IN THIS WORK AND THOSE REPORTED PREVIOUSLY

Reference antenna	Antenna type	Tilted beam	Operating frequency (GHz)	Antenna size (λ_0^2)	Antenna profile (λ_0)	Aperture efficiency	Realized Gain
[18]	Transmitarray	Yes	9.15−10.45	16	3.5	40.2%	19.2−20.2 dBic
[20]	Reflectarray	Yes	55−65	121	5.5	40.5%	25.0−27.9 dBi
[26], Switched beam	Fabry-Perot cavity	Yes	57−63	58	1.4	20%	14−15.8 dBi
[28], Tilted CP beam	Modulated metasurface	Yes	8.425	57.45π	0.04	50.9%	30.0 dBic
[30]	Radial line slot	Yes	17.3	60.6π	0.18	50.8%	30.7 dBi
[33], Linear polarization	TE_{330}-mode cavity	No	29−35	2.33	0.17	76.5%	10.7−13.8 dBi
[36], Antenna element	TE_{560}-mode cavity	No	92.74−96.87	7.1	0.16	49.4%	16.44 dBi
[38], Antenna B.2	Cavity-feed patch array	No	9.48	25	1.05	59%	22.8 dBi
[39], 4×4 array	Cavity-feed patch array	No	30	7.5	0.13	33.6%	15 dBi
This work, Single tilted beam	$TE_{(10)(11)(0)}$-mode cavity with phased patch surface	Yes	10.5	54.94	0.4	56.6%	25.3 dBi

bandwidths. As indicated in the table, the antenna developed in this work has performance characteristics comparable to those systems. Moreover, they all have a low profile, i.e., their height is less than $0.5\lambda_0$; and they all radiate beams with a peak realized gain that is larger than 25 dBi/dBic.

It must be emphasized that all of the previously reported cavity antennas in [33] and [36], [38], [39] only radiate broadside beams. The slots etched with proper offsets into the top surface of the resonant higher-order mode cavities in [33] and [36] achieve focused high-gain broadside beams. The slot-based higher-order-mode resonant cavities in [38], [39] drive the principal radiators located above their slots, an array of half-wavelength-sized patches; but they too only radiate high gain broadside beams. The phase-control surface, which was the innovative contribution of this work, clearly enhances the functionality of existing overmoded cavity antennas by facilitating their ability to radiate tilted beams. It is noted that the beam-tilt range of the overmoded cavity antennas augmented with the phase-control surface is dependent on the electrical distance between their slot elements. Thus, it is limited in these slot-based air-filled overmoded cavity designs by the fact that the physical distance between their slots is specifically determined by the wavelength of the resonant mode excited in the cavity. If the cavity is filled with a dielectric substrate, the wavelength in the cavity will then be decreased. The surface of the cavity is also modified so that the distance of separation between the slots matches this new half-wavelength. The electrical distance between the slots is then decreased and, hence, the beam steering range can be increased.

Although changing patch dimensions for phase control has been widely reported in relation to metamaterial-based and transmitarray/reflectarray antennas [18], [20], [37], [45], there are significant differences between those methods and the one developed in this work. Because they usually employ a single source to illuminate a large patch-based phase-control surface and the surface is in the far-field of that source, their phase behaviors are determined by illuminating it with a transverse electromagnetic (TEM) plane wave. The resulting transmission or reflection coefficients are monitored to determine the variations in the phase response for different patch sizes. In contrast, our slot-based resonant cavity array serves as the base "excitation" of the phase control surface augmenting it. Each slot has a patch over it in its near field. The near-field coupling of the slot and the augmented patch controls the resulting phase response of this combination. A TE_{110}-mode single-slot cavity antenna and its augmentation with a substrate suspended patch over it are introduced and employed to determine the phase of the electric fields which this combined system radiates into its far-field. One cannot get the correct phase response if the analysis with the TEM illumination used in the metamaterial and transmitarray/reflectarray elements is adopted. It is recalled that a 131.9° phase variation could be achieved by changing only the patch length in our work. This phase range was then doubled to 263.8° when the slots were properly offset from their subsection centers. Nevertheless, it is not feasible to double the phase range by changing the slot offsets in those reported metamaterial-based and transmitarray/reflectarray antennas.

B. Impedance Bandwidth

While the very high-Q overmoded cavity design led to a narrow bandwidth, one could improve it by using a multiple feed technique. For example, the slot-based overmoded cavity antenna with a single tilted-beam can be modified by replacing the single waveguide feed with two slot-coupled microstrip line feeds. Fig. 16 (a) shows the bottom view of this system. The two slots are etched into the bottom of the overmoded cavity and are located symmetrically along the y-axis at the positions x_m = 38.4 mm. The length and width of both slots are, respectively, L_s = 18 mm and W_s = 5 mm. The two microstrip feed lines are symmetrically printed on the bottom surface of a F4BM-2 substrate disk whose radius is the same as the cavity and whose top surface is attached to its bottom. The substrate height is 1.5 mm. The length and width of both microstrip feedlines are, respectively, L_f = 60.6 mm and W_f = 3 mm. They are fed at Port 1 and Port 2 with the same amplitudes but opposite phase values.

Fig. 17 shows the simulated $|S_{11}|$ values of this two-port design as a function of the source frequency. The simulated

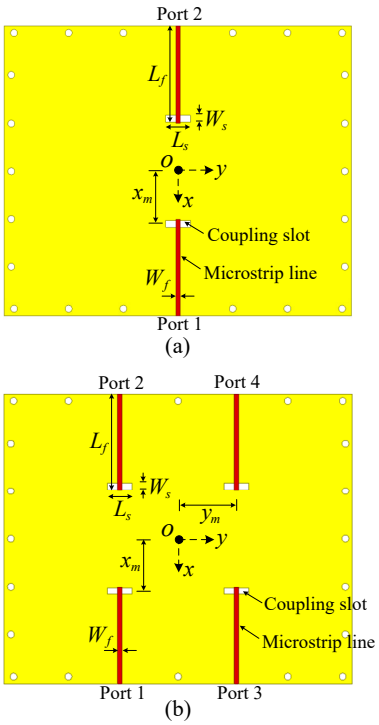

Fig. 16. Bottom view of the patch-augmented slot-based overmoded cavity antenna with microstrip line feeds. (a) Two microstrip feeds. (b) Four microstrip feeds. (The substrates are not present for visual purposes.)

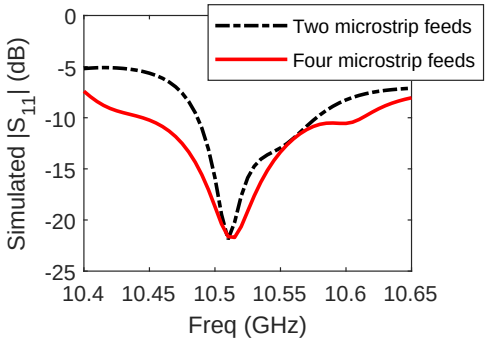

Fig. 17. Simulated $|S_{11}|$s of the patch-augmented slot-based overmoded cavity antennas with microstrip line feeds.

$|S_{11}| \leq -10$ dB bandwidth is 90 MHz, from 10.49 to 10.58 GHz. The simulated peak realized gain value is 25.6 dBi, which is around 0.6 dBi lower than the value, 26.2 dBi, of the original design. Thus the bandwidth has been improved three-fold at the cost of 0.6 dBi.

The bandwidth can be further increased by increasing the number of slots and their microstrip feed lines. Fig. 16 (b) illustrates a four-port design. The slots are now located at the symmetric positions (x_m,y_m) = ($\pm$38.4 mm, $\pm$42.54 mm). The lengths and widths of the slots and their microstrip feed lines are the same as in the two-port design. All of the four ports are excited with the same amplitude, while the excitation phase values for Port 1 to Port 4 are 0°, 180°, 0°, 180°, respectively. Fig. 17 also shows the simulated $|S_{11}|$ values of this four-port design as a function of the source frequency. Its $-$10-dB impedance bandwidth has been increased to 160 MHz, from 10.45 to 10.61 GHz. On the other hand, the simulated peak realized gain value has been reduced further to 24.5 dBi, 1.7 dBi lower than the original single port design's value. Thus, one finds that there are tradeoffs when designing a slot-based overmoded cavity antenna among its peak gain, impedance bandwidth, and fabrication complexity.

V. Conclusion

A phase-control surface was developed to enable the realization of high-gain tilted beams from slot-based overmoded cavity antennas. A TE_{110}-mode single-slot cavity antenna, which is effectively one half-wavelength subsection of the base higher-order $TE_{(10)(11)(0)}$-mode cavity antenna, was augmented with a closely-spaced patch. The fields it radiates were monitored to understand their phase behavior when the patch length and slot offset were varied. A systemic process was provided to design a phase-control surface that could be easily integrated with the base antenna to achieve titled beams. It can be generalized to deal with a variety of different cavity shapes and their resonant modes.

The efficacy of this engineered phase-control surface was verified by developing and testing a system that radiates a single beam tilted 30° from broadside and another one that radiates two beams respectively pointed at $-10°$ and 20°. The measured results of both low profile systems confirmed their simulated characteristics. These enhanced functionality, slot-based overmoded cavity antennas are promising candidates for a variety of current and future wireless systems.

References

[1] Q. Zhu, K. B. Ng, C. H. Chan, and K. M. Luk, "Substrate-integrated-waveguide-fed array antenna covering 57-71 GHz band for 5G applications," *IEEE Trans. Antennas Propag.*, vol. 65, no. 12, pp. 6298–6306, Dec. 2017.

[2] O. Jo, J. Kim, J. Yoon, D. Choi, and W. Hong, "Exploitation of dual-polarization diversity for 5G millimeter-wave MIMO beamforming systems," *IEEE Trans. Antennas Propag.*, vol. 65, no. 12, pp. 6646–6655, Dec. 2017.

[3] O. Quevedo-Teruel, M. Ebrahimpouri, and F. Ghasemifard, "Lens antennas for 5G communications systems," *IEEE Commun. Mag.*, vol. 56, no. 7, pp. 36–41, Jul. 2018.

[4] J. Wang *et al.*, "Metantenna: When metasurface meets antenna again," *IEEE Trans. Antennas Propag.*, vol. 68, no. 3, pp. 1332–1347, 2020.

[5] R. J. Mailloux, *Phased Array Antenna Handbook*. London, UK: Wendt Library, 2005.

[6] B. Fuchs and S. Rondineau, "Array pattern synthesis with excitation control via norm minimization," *IEEE Trans. Antennas Propag.*, vol. 64, no. 10, pp. 4228–4234, Oct. 2016.

[7] Y. Liu *et al.*, "Linearly polarized shaped power pattern synthesis with sidelobe and cross-polarization control by using semidefinite relaxation," *IEEE Trans. Antennas Propag.*, vol. 66, no. 6, pp. 3207–3212, Jun. 2018.

[8] J. Huang *et al.*, "A new compact and high gain circularly-polarized slot antenna array for Ku-band mobile satellite TV reception," *IEEE Access*, vol. 5, pp. 6707–6714, 2017.

[9] Y. Miura, J. Hirokawa, M. Ando, Y. Shibuya, and G. Yoshida, "Double-layer full-corporate-feed hollow-waveguide slot array antenna in the 60-GHz band," *IEEE Trans. Antennas Propag.*, vol. 59, no. 8, pp. 2844–2851, Aug. 2011.

[10] J. Liu, A. Vosoogh, A. U. Zaman, and J. Yang, "Design and fabrication of a high-gain 60-GHz cavity-backed slot antenna array fed by inverted microstrip gap waveguide," *IEEE Trans. Antennas Propag.*, vol. 65, no. 4, pp. 2117–2122, Apr. 2017.

[11] D. Kim, M. Zhang, J. Hirokawa, and M. Ando, "Design and fabrication of a dual-polarization waveguide slot array antenna with high isolation and high antenna efficiency for the 60 GHz band," *IEEE Trans. Antennas Propag.*, vol. 62, no. 6, pp. 3019–3027, Jun. 2014.

[12] G. Sun and H. Wong, "A planar millimeter-wave antenna array with pillbox distributed network," *IEEE Trans. Antennas Propag.*, pp. 1–1, 2020.
[13] A. H. Abdelrahman, F. Yang, A. Z. Elsherbeni, P. Nayeri, and C. A. Balanis, *Analysis and Design of Transmitarray Antennas*. San Francisco, CA, USA: Morgan & Claypool, 2017.
[14] E. Erfani, M. Niroo-Jazi, and S. Tatu, "A high-gain broadband gradient refractive index metasurface lens antenna," *IEEE Trans. Antennas Propag.*, vol. 64, no. 5, pp. 1968–1973, May 2016.
[15] Y. Hou, L. Chang, Y. Li, Z. Zhang, and Z. Feng, "Linear multibeam transmitarray based on the sliding aperture technique," *IEEE Trans. Antennas Propag.*, vol. 66, no. 8, pp. 3948–3958, Aug. 2018.
[16] S. H. Ramazannia Tuloti, P. Rezaei, and F. Tavakkol Hamedani, "High-efficient wideband transmitarray antenna," *IEEE Antennas Wireless Propag. Lett.*, vol. 17, no. 5, pp. 817–820, May 2018.
[17] Q. Luo *et al.*, "A hybrid design method for thin-panel transmitarray antennas," *IEEE Trans. Antennas Propag.*, vol. 67, no. 10, pp. 6473–6483, Oct. 2019.
[18] F. Zhang, G. Yang, and Y. Jin, "Low-profile circularly polarized transmitarray for wide-angle beam control with a third-order meta-FSS," *IEEE Trans. Antennas Propag.*, vol. 68, no. 5, pp. 3586–3597, 2020.
[19] H. Yang *et al.*, "A 1-bit 10×10 reconfigurable reflectarray antenna: Design, optimization, and experiment," *IEEE Trans. Antennas Propag.*, vol. 64, no. 6, pp. 2246–2254, Jun. 2016.
[20] G. Wu *et al.*, "High-gain filtering reflectarray antenna for millimeter-wave applications," *IEEE Trans. Antennas Propag.*, vol. 68, no. 2, pp. 805–812, Feb. 2020.
[21] G. Wu, S. Qu, S. Yang, and C. H. Chan, "Low-cost 1-D beam-steering reflectarray with $\pm$ 70° scan coverage," *IEEE Trans. Antennas Propag.*, pp. 1–1, 2020.
[22] A. Epstein, J. P. S. Wong, and G. V. Eleftheriades, "Cavity-excited Huygens' metasurface antennas for near-unity aperture illumination efficiency from arbitrarily large apertures," *Nat. Commun.*, vol. 7, p. 10360, Jan. 2016.
[23] Y. Ge, Z. Sun, Z. Chen, and Y. Chen, "A high-gain wideband low-profile Fabry-Perot resonator antenna with a conical short horn," *IEEE Antennas Wireless Propag. Lett.*, vol. 15, pp. 1889–1892, 2016.
[24] M. U. Afzal and K. P. Esselle, "Steering the beam of medium-to-high gain antennas using near-field phase transformation," *IEEE Trans. Antennas Propag.*, vol. 65, no. 4, pp. 1680–1690, Apr. 2017.
[25] N. Nguyen-Trong, H. H. Tran, T. K. Nguyen, and A. M. Abbosh, "Wideband Fabry-Perot antennas employing multilayer of closely spaced thin dielectric slabs," *IEEE Antennas Wireless Propag. Lett.*, vol. 17, no. 7, pp. 1354–1358, Jul. 2018.
[26] Q. Guo and H. Wong, "Wideband and high-gain Fabry-Perot cavity antenna with switched beams for millimeter-wave applications," *IEEE Trans. Antennas Propag.*, vol. 67, no. 7, pp. 4339–4347, Jul. 2019.
[27] ——, "A millimeter-wave Fabry-Perot cavity antenna using Fresnel zone plate integrated PRS," *IEEE Trans. Antennas Propag.*, vol. 68, no. 1, pp. 564–568, Jan 2020.
[28] G. Minatti *et al.*, "Modulated metasurface antennas for space: Synthesis, analysis and realizations," *IEEE Trans. Antennas Propag.*, vol. 63, no. 4, pp. 1288–1300, 2015.
[29] ——, "Synthesis of modulated-metasurface antennas with amplitude, phase, and polarization control," *IEEE Trans. Antennas Propag.*, vol. 64, no. 9, pp. 3907–3919, 2016.
[30] J. I. Herranz, A. Valero-Nogueira, F. Vico, and V. M. Rodrigo, "Optimization of beam-tilted linearly polarized radial-line slot-array antennas," *IEEE Antennas Wireless Propag. Lett.*, vol. 9, pp. 1165–1168, 2010.
[31] A. Akiyama *et al.*, "High gain radial line slot antennas for millimetre wave applications," *IEE Proc. Microw., Antennas Propag.*, vol. 147, no. 2, pp. 134–138, Apr. 2000.
[32] T. Nguyen, H. Ueda, J. Hirokawa, and M. Ando, "A radial line slot antenna for an elliptical beam," *IEEE Trans. Antennas Propag.*, vol. 60, no. 12, pp. 5531–5537, Dec. 2012.
[33] W. Han, F. Yang, J. Ouyang, and P. Yang, "Low-cost wideband and high-gain slotted cavity antenna using high-order modes for millimeter-wave application," *IEEE Trans. Antennas Propag.*, vol. 63, no. 11, pp. 4624–4631, Nov. 2015.
[34] W. Han, F. Yang, R. Long, L. Zhou, and F. Yan, "Single-fed low-profile high-gain circularly polarized slotted cavity antenna using a high-order mode," *IEEE Antennas Wireless Propag. Lett.*, vol. 15, pp. 110–113, 2016.
[35] M. Asaadi and A. Sebak, "High-gain low-profile circularly polarized slotted SIW cavity antenna for MMW applications," *IEEE Antennas Wireless Propag. Lett.*, vol. 16, pp. 752–755, 2017.
[36] Q. Yuan, Z. Hao, K. Fan, and G. Q. Luo, "A compact W-band substrate-integrated cavity array antenna using high-order resonating modes," *IEEE Trans. Antennas Propag.*, vol. 66, no. 12, pp. 7400–7405, Dec. 2018.
[37] H. Li, G. Wang, X. Gao, J. Liang, and H. Hou, "A novel metasurface for dual-mode and dual-band flat high-gain antenna application," *IEEE Trans. Antennas Propag.*, vol. 66, no. 7, pp. 3706–3711, 2018.
[38] A. M. Jassim and H. D. Hristov, "Cavity feed technique for slot-coupled microstrip patch array antenna," *IEE Proc. Microwave Antennas Propag.*, vol. 142, no. 6, pp. 452–456, 1995.
[39] B. T. Malik, V. Doychinov, S. A. R. Zaidi, N. Somjit, I. D. Robertson, and C. W. Turner, "Higher-order mode substrate integrated waveguide cavity excitation for microstrip patch antenna arrays at 30-GHz," *J. Phys. Commun.*, vol. 3, no. 1, p. 015017, Jan. 2019.
[40] C.-Y. Huang, J.-Y. Wu, and K.-L. Wong, "Slot-coupled microstrip antenna for broadband circular polarisation," *Electron. Let.*, vol. 34, no. 9, pp. 835–836, Apr. 1998.
[41] K.-L. Wong, H.-C. Tung, and T.-W. Chiou, "Broadband dual-polarized aperture-coupled patch antennas with modified H-shaped coupling slots," *IEEE Trans. Antennas Propag.*, vol. 50, no. 2, pp. 188–191, Feb. 2002.
[42] T. H. Jang, H. Y. Kim, D. M. Kang, S. H. Kim, and C. S. Park, "60 GHz low-profile, wideband dual-polarized U-slot coupled patch antenna with high isolation," *IEEE Trans. Antennas Propag.*, vol. 67, no. 7, pp. 4453–4462, 2019.
[43] R. F. Harrington, *Time-Harmonic Electromagnetic Fields*. New York, NY, USA: McGraw-Hill, 1961.
[44] R. J. Mailloux, *Phased Array Antenna Handbook*. Artech House, USA, 2017.
[45] T. Cai, G. Wang, X. Fu, J. Liang, and Y. Zhuang, "High-efficiency metasurface with polarization-dependent transmission and reflection properties for both reflectarray and transmitarray," *IEEE Trans. Antennas Propag.*, vol. 66, no. 6, pp. 3219–3224, 2018.

Shu-Lin Chen (M'20) was born in Hubei Province, China. He received the B.S. degree in electrical engineering from Fuzhou University (FZU), China, in 2012; the M.S. degree in electromagnetic field and microwave technology from Xiamen University (XMU), China, in 2015; and the Ph.D. degree in engineering from the University of Technology Sydney (UTS), Australia, in 2019.

From April to July 2019, he was a Visiting Scholar with the State Key Laboratory of Terahertz and Millimeter Waves, City University of Hong Kong (CityU). Since September 2019, he has been a post-doctoral research associate with the Global Big Data Technologies Centre (GBDTC), UTS, Australia. His research interests include reconfigurable antennas, leaky-wave antennas, and millimeter-wave antennas. He was a finalist of ISAP 2017 best paper competition, and his paper was listed as an Honorary Mention in APS-URSI 2017.

Yanhui Liu (M'2015-SM'2019) received the B.S. and Ph.D. degrees both in electrical engineering from the University of Electronic Science and Technology of China (UESTC) in 2004 and 2009, respectively.

From September 2007 to June 2009, he was a Visiting Scholar in the Department of Electrical Engineering at Duke University, Durham, NC. In July 2011, he joined in the Department of Electronic Science, Xiamen University, China, where he was lately promoted as a Full Professor. From September to December in 2017, he was a Visiting Professor at State Key Laboratory of Millimeter Waves in City University of Hong Kong. From December 2017 to December 2019, he had been with Global Big Data Technologies Centre, University of Technology Sydney (UTS) as a Visiting Professor/Research Principal. From November 2019, he has been a Professor at UESTC. He received the UESTC Outstanding Graduate Award in 2004, and the Excellent Doctoral Dissertation Award of Sichuan Province of China in 2011. He has authored and co-authored over 160 peer-reviewed journal and conference papers including 95 SCI-indexed papers. He holds 21 Chinese invention patents in antennas and applied electromagnetics.

Dr. Liu is serving as a reviewer for a dozen of SCI-indexed journals. Since 2018, he has served as an Associate Editor for the IEEE Access. He has served many times as TPC member/reviewer/session chair in a number of international conferences in the field of antennas and propagation. His research interests include antenna array design, reconfigurable antennas, and electromagnetic scattering and imaging.

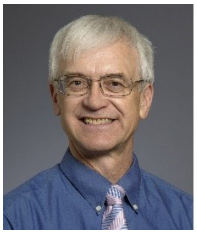

Richard W. Ziolkowski (Life Fellow, IEEE) received the B. Sc. (magna cum laude) degree (Hons.) in physics from Brown University, Providence, RI, USA, in 1974; the M.S. and Ph.D. degrees in physics from the University of Illinois at Urbana-Champaign, Urbana, IL, USA, in 1975 and 1980, respectively; and an Honorary Doctorate degree from the Technical University of Denmark, Kongens Lyngby, Denmark in 2012.

He is currently a Distinguished Professor in the Global Big Data Technologies Centre in the Faculty of Engineering and Information Technologies (FEIT) at the University of Technology Sydney, Ultimo NSW Australia. He became a Professor Emeritus at the University of Arizona in 2018, where he was a Litton Industries John M. Leonis Distinguished Professor in the Department of Electrical and Computer Engineering in the College of Engineering and was also a Professor in the College of Optical Sciences. He was the Computational Electronics and Electromagnetics Thrust Area Leader with the Engineering Research Division of the Lawrence Livermore National Laboratory before joining The University of Arizona, Tucson, AZ, USA, in 1990. His current research interests include the application of new mathematical and numerical methods to linear and nonlinear problems dealing with the interaction of electromagnetic and acoustic waves with complex linear and nonlinear media, as well as metamaterials, metamaterial-inspired structures, nano-structures, and other classical and quantum applications-specific configurations.

Prof. Ziolkowski is the recipient of the 2019 IEEE Electromagnetics Award (IEEE Technical Field Award). He is a Fellow of the Optical Society of America (OSA, 2006) and the American Physical Society (APS, 2016). He served as the President of the IEEE Antennas and Propagation Society (AP-S) in 2005 and has had many other AP-S leadership roles. He is also actively involved with the URSI, EurAPP, OSA and SPIE professional societies. He was the 2014-2015 Australian DSTO Fulbright Distinguished Chair in Advanced Science and Technology. He was a 2014 Thomas-Reuters Highly Cited Researcher.

Zheng Li (M'15) received the B.S. degree in physics and the Ph.D. degree in Electrical Engineering from Beijing Jiaotong University, Beijing, China, in 2006 and 2012, respectively.

From 2008 to 2009, he was a Visiting Student with Pennsylvania State University, State College, PA, USA. In 2012, he joined the Faculty of the Department of Electrical Engineering, Beijing Jiaotong University, where he became a Professor in 2019. From 2017 to 2018, he was a Visiting Professor with the Global Big Data Technologies Centre, University of Technology Sydney, Ultimo, NSW, Australia. His current research interests include electrically beam-scanning antennas and leaky-wave structures.

Y. Jay Guo (Fellow'2014) received a Bachelor Degree and a Master Degree from Xidian University in 1982 and 1984, respectively, and a PhD Degree from Xian Jiaotong University in 1987, all in China. His research interest includes antennas, mm-wave and THz communications and sensing systems as well as big data technologies. He has published four books and over 600 research papers including over 280 IEEE Transactions papers, and he holds 26 patents. He is a Fellow of the Australian Academy of Engineering and Technology, a Fellow of IEEE and a Fellow of IET, and was a member of the College of Experts of Australian Research Council (ARC, 2016-2018). He has won a number of most prestigious Australian Engineering Excellence Awards (2007, 2012) and CSIRO Chairman's Medal (2007, 2012). He was named one of the most influential engineers in Australia in 2014 and 2015, respectively, and one of the top researchers across fields in Australia in 2020.

He is a Distinguished Professor and the Director of Global Big Data Technologies Centre (GBDTC) at the University of Technology Sydney (UTS), Australia. Prior to this appointment in 2014, he served as a Director in CSIRO for over nine years. Before joining CSIRO, he held various senior technology leadership positions in Fujitsu, Siemens and NEC in the U.K.

Prof Guo has chaired numerous international conferences and served as guest editors for a number of IEEE publications. He is the Chair of International Steering Committee, International Symposium on Antennas and Propagation (ISAP). He has been the International Advisory Committee Chair of IEEE VTC2017, General Chair of ISAP2022, ISAP2015, iWAT2014 and WPMC'2014, and TPC Chair of 2010 IEEE WCNC, and 2012 and 2007 IEEE ISCIT. He served as Guest Editor of special issues on "*Low-Cost Wide-Angle Beam Scanning Antennas*", "*Antennas for Satellite Communications*" and "*Antennas and Propagation Aspects of 60-90 GHz Wireless Communications*," all in IEEE Transactions on Antennas and Propagation, Special Issue on "*Communications Challenges and Dynamics for Unmanned Autonomous Vehicles*," IEEE Journal on Selected Areas in Communications (JSAC), and Special Issue on ''*5G for Mission Critical Machine Communications*", IEEE Network Magazine.